LANGMUIR Article
Cite This: Langmuir 2017, 33, 14325−14331
pubs.acs.org/Langmuir

Dewetting-Induced Photoluminescent Enhancement of Poly(lauryl methacrylate)/Quantum Dot Thin Films

Jeffrey Geldmeier, Lexy Rile, Young Jun Yoon, Jaehan Jung, Zhiqun Lin, and Vladimir V. Tsukruk*

School of Materials Science and Engineering, Georgia Institute of Technology, Atlanta, Georgia 30332-0245, United States

Supporting Information

ABSTRACT: A new method for enhancing photoluminescence from quantum dot (QD)/polymer nanocomposite films is proposed. Poly(lauryl methacrylate) (PLMA) thin films containing embedded QDs are intentionally allowed to undergo dewetting on substrates by exposure to a nonsolvent vapor. After controlled dewetting, films exhibited typical dewetting morphologies with increased amounts of scattering that served to outcouple photoluminescence from the film and reduce internal light propagation within the film. Up to a 5-fold enhancement of the film emission was achieved depending on material factors such as the initial film thickness and QD concentration within the film. An increase in initial film thickness was shown to increase the dewetted maximum feature size and its characteristic length until a critical thickness was reached where dewetting became inhibited. A unique light exposure-based photopatterning method is also presented for the creation of high contrast emissive patterns as guided by spatially controlled dewetting.

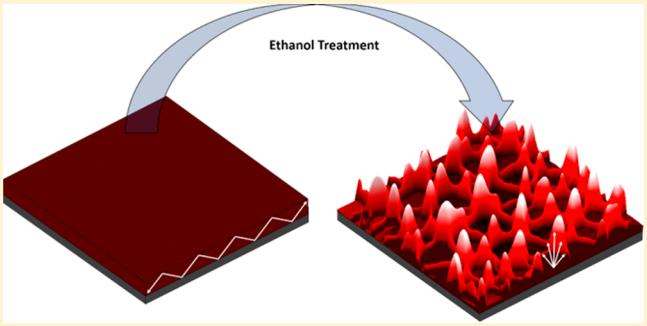

INTRODUCTION

Synthesis of semiconductor materials on the nanoscale has led to the emergence of nanostructures with novel and tunable optical properties due to the quantum confinement of their energy levels below the Bohr exciton radius into discrete band gaps.[1] In particular, quantum dots (QDs) are well-known 0D semiconducting photoluminescent (PL) nanoparticles, typically in the size range of 5−10 nm, that are desirable for many optical applications due to their narrow emission profile, broadband absorption, and size-dependent tunable band gap.[1−4] Furthermore, core/shell and alloyed QDs are resistant to many chemical and oxidative agents that may pose a problem for traditional organic molecules and dyes.[3,5−7] Efforts to increase their intrinsic brightness have also resulted in QDs with quantum yields approaching unity, although their outcoupling behavior decreases drastically in films and other solid state structures.[8] These assorted advantages have already led to QDs being adopted for commercial applications in devices such as biological labels,[9] light-emitting diodes (LEDs),[10,11] solar cells,[12] and lasers,[13] and further efforts to improve their photoluminescence (PL) in solid state films or devices would broaden their future applications.

Several methods have been developed for the furthered PL enhancement of emissive QDs and their composite films beyond improving their intrinsic properties. Designing photonic crystals with photonic band gaps at the emission wavelength can lead to enhancement factors as high as 20 due to the negligible absorption or transmission that can occur at the crystal surfaces.[14−16] Purcell antennas can be formed using noble metal nanoparticles or shells that can enhance the PL of emitters as well, although this approach is very hard to control over large surface areas due to coupling interactions between nanoparticles that may shift or broaden their plasmon resonance, and specific approaches must be tailored for different emission wavelengths.[17−21]

Alternatively, introducing predesigned scattering sites such as meshed surfaces,[22] microspheres,[23] and nanoparticles[24] has also proven to be an effective way of allowing more light outcoupling and higher PL by improving emission outcoupling to the far field and by reducing the amount of waveguided modes within the films. Recently, Prins et al. demonstrated a 6-fold enhancement of QD PL normal to the surface by fabricating bull's-eye gratings that resulted in constructive Bragg interference.[25] These approaches are more universal in nature and have been used with a wide variety of surfaces and architectures.

One method traditionally not considered to date for introducing PL enhancement is the intentional dewetting-induced patterning of QD/polymer thin films. Below approximately 100 nm, film interfaces with substrates are dominated by intermolecular interactions that are highly sensitive to perturbations in the environment.[26,27] Depending on the polymer film/substrate and polymer film/air interface energy balance, films may be stable, unstable, or metastable.[28,29] For unstable films below a critical thickness, thermal annealing of a thin film polymer film can induce spinodal dewetting of

Received: September 28, 2017
Revised: November 7, 2017
Published: November 27, 2017

ACS Publications © 2017 American Chemical Society

DOI: 10.1021/acs.langmuir.7b03400
Langmuir 2017, 33, 14325−14331

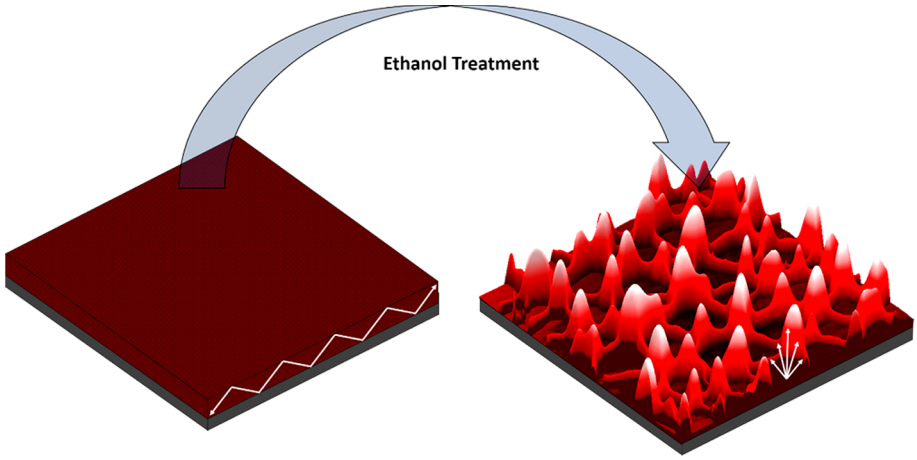

Figure 1. Schematic of the polymer/QD film morphology transformation as a result of controlled dewetting.

films into patterns with a characteristic length scale. Besides directly raising the temperature above the glass transition, polymer dewetting can be induced by immersing it in a poor or nonsolvent.[27,30] Solvent-assisted dewetting has also been shown to be a product of stronger polar interactions, rather than weak van der Waals forces that accompany thermal dewetting, that promote quicker dewetting and smaller characteristic feature lengths of the dewetted domains.[27,31] While the mechanisms behind the dewetting process have been the subject of intensive research for decades, few studies have investigated the integrated optical properties of such dewetted films with incorporated optically active components such as QDs.

In this work, a facile, scalable, and quick method of enhancing the PL of polymer/QD nanocomposite films is presented. By intentionally dewetting composite QD-containing poly(lauryl methacrylate) (PLMA) films with ethanol vapor, a high concentration of light-scattering sites from the emergence of nanoscale domains is induced, thereby resulting in a significant increase in the apparent emissive intensity of the films (Figure 1). Strong and stable PL enhancement factors of up to 5 over large areas (centimeter size) are achieved using this method without the use of further cost- or time-intensive processes.

EXPERIMENTAL DETAILS

Materials. PLMA (M_W = 570 000), ethanol, cadmium oxide (CdO), tri*n*-octylphosphine (TOP, 90%), and tributylphosphine (TBP, >93.5%) were obtained from Sigma-Aldrich. Selenium powder (Se, 99.999%), 1-tetradecylphosphonic acid (TDPA, 98%), tri-*n*-octylphosphine oxide (TOPO, 90%), diethylzinc (15 wt % in hexane), and hexane were obtained from Alfa Aesar. Hexadecylamine (HDA, 90%) and bis(trimethylsilyl) sulfide (95%) were obtained from TCI. Toluene was obtained from BDH Chemicals. All chemicals were used as received.

Synthesis of CdSe/$Cd_{1-x}Zn_xSe_{1-y}S_y$ Core/Graded Shell QDs. Red core/graded shell CdSe/$Cd_{1-x}Zn_xSe_{1-y}S_y$ QDs were synthesized by modifying areported method.[32] Briefly, 1 mmol of CdO, 2 mmol of $Zn(acetate)_2$, 5 mL of oleic acid, and 15 mL of 1-octadecene were inserted into a three-neck flask. The mixture was then degassed at 150 °C for 1 h. The reaction was heated to 300 °C under Ar. At the elevated temperature (300 °C), 0.2 mL of 1 M Se/TOP solution was rapidly injected. After 5 min, 0.3 mL of dodecanethiol was added dropwise. The solution was kept at 300 °C for 20 min followed by injection of 1 mL of 2 M S/TOP solution. The reaction was allowed to proceed at 300 °C for 10 min, and then the reaction was stopped by removing the heating mantle. Ten ml of hexane was added to the solution once the temperature reached 70 °C. The resulting QDs were approximately 8.1 ± 0.3 nm in size based on transmission electron microscopy measurements from a previous study.[32]

PLMA/QD Composite Films. To prepare PLMA/QD composite films, 50 μL of QDs in toluene was first crashed out by adding acetone and centrifuging at 12 000 rpm for 10 min. After centrifugation, the supernatant was drained and 120 μL of PLMA of varying wt % (0.25−2%) in toluene was added. QDs were dispersed in solution by rotomixing for 30 s followed by sonication for 10 s. Longer sonication times were found to promote aggregation of the QDs. Films were then cast from solution onto silicon wafers by spin coating at 3000 rpm for 30 s.

Controlled Dewetting Procedure. PLMA/QD films were dewet immediately after being cast onto silicon substrates, as long dwell times promoted film adhesion to the substrate and resulted in no dewetting behavior. Films were then sprayed with ethanol using a spray gun (Iwata HP-CS) at 10 psi for 1 s in such a way that the substrate was only misted and so that the ethanol evaporated quickly. Longer evaporation times were found to lead to complete delamination of the film or irregular dewetting behavior. After treatment, films became visibly blue. For photopatterning beforehand, films were placed under a mask and exposed to a 120 W mercury arc lamp (Lumen Dynamics, X-cite series, 120Q) for 30 min.

Characterization. Atomic force microscopy (AFM) was conducted on PLMA and PLMA/QD composite films using a Dimension 3000 (Digital Instruments) instrument in tapping mode similarly to previous experiments.[33] Briefly, scans were performed at a rate of 1 Hz for 2 × 2 μm^2 and 20 × 20 μm^2 surface areas at a resolution of 512 × 512 pixels. Silicon nitride tips (MikroMasch) with a spring constant of 7 N/m and a resonant frequency of approximately 140 kHZ were used for imaging.

Spectroscopic ellipsometry was conducted using a M-2000U Woollam ellipsometer to measure PLMA film thicknesses. Reflection data was collected at incident angles of 65°, 70°, and 75°, and the film was modeled as a Cauchy layer. Photoluminescence spectra were obtained from the PLMA/QD composite films using a Cytoviva hyperspectral imaging system with a diffraction grating spectrophotometer wavelength range of 400−1000 nm. Here, 10× (NA: 0.30) and 50× (NA: 0.80) objectives were used to collect both scattering and PL data. Illumination was conducted using the same mercury arc lamp with a 120 W power used for photopatterning. PL imaging was performed using an additional bandpass filter (450−490 nm), a dichroic mirror that reflects light below 495 nm, and a long-pass filter that transmits optical wavelengths above 500 nm. Scans were taken with a 0.5 s integration time, and at least three scans were conducted at different spots for each sample to obtain an average PL value.

RESULTS AND DISCUSSION

PLMA/QD Film Morphology. PLMA/QD films were first characterized before dewetting to examine their thicknesses and

DOI: 10.1021/acs.langmuir.7b03400
Langmuir 2017, 33, 14325−14331

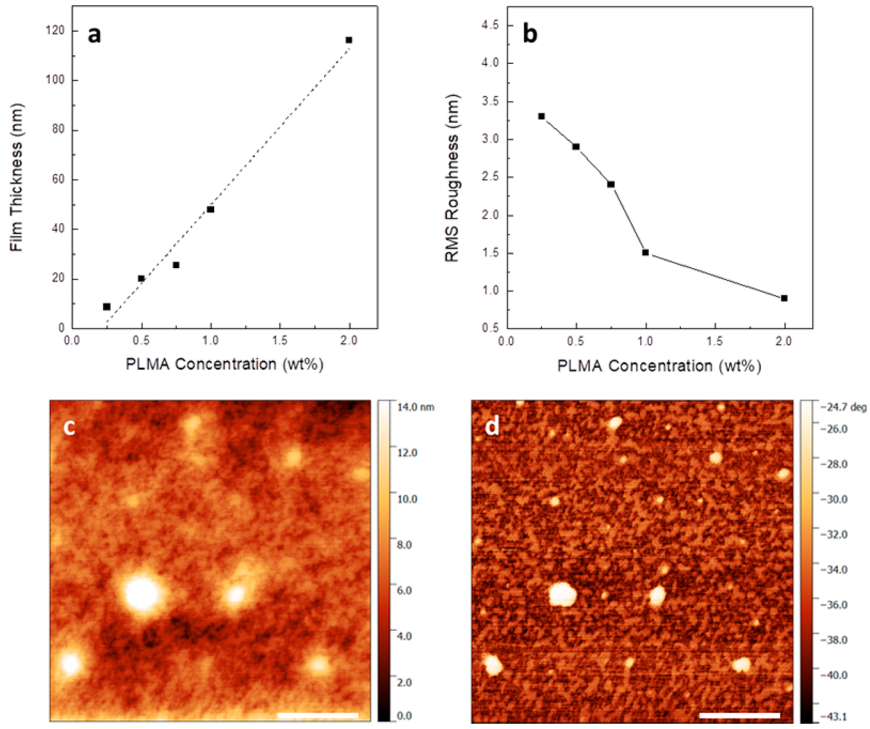

Figure 2. (a) PLMA/QD composite film thickness as a function of PLMA wt %. (b) Film surface roughness as a function of PLMA wt %. (c) AFM topography of a PLMA/QD film with a 9 nm average height. (d) Corresponding phase image. Scale bars are 500 nm.

morphologies prior to ethanol exposure. The films were found to scale roughly linearly in thickness with the PLMA concentration in solution as expected, with average thicknesses of 9, 20, 26, 48, and 116 nm for respective PLMA solution concentrations of 0.25, 0.5, 0.75, 1, and 2 wt % (Figure 2a). The corresponding RMS surface roughness was found to decrease from 3.3 to 0.9 nm for a 4 μm^2 surface area as the film thickness increased from 9 to 116 nm, which is most likely due to QD aggregations being more fully encompassed within the films (Figure 2b). In a 20 nm thick film for instance, PLMA/QD film surfaces appear mostly uniform but do display some aggregation and a 2.9 nm RMS roughness over a 4 μm^2 surface area (Figure 2c). Corresponding AFM phase images also reveal modest phase separation within the film between the PLMA and QDs (Figure 2d).

Upon 1 s exposure to ethanol vapor and subsequent drying, PLMA/QD film morphologies were found to dewet immediately and in a manner dependent on the initial thicknesses of the films. In contrast, thermally annealed films dewet over much longer time periods of minutes or hours. It should also be noted that films aged >24 h in air became stable, most likely due to the evaporation of residual solvent, and did not display dewetting behavior.

The 9 nm film features could not be resolved optically, although the dark field image appeared blue and is composed of many scattering sites (Figure 3a). AFM images reveal a droplet morphology commonly associated with the spinodal dewetting behavior of very thin films (Figure 3b).[29,34] Micrometer-sized "coffee ring" edges are apparent as well in Figure 3a that can be attributed to the ethanol vapor droplet evaporation, although no differences in morphology or QD concentration were seen between ring centers and edges.

The 20, 26, and 48 nm PLMA/QD films all displayed conventional network-like Voronoi patterns consistent with hole nucleation dewetting that occurs for thicker films (Figures

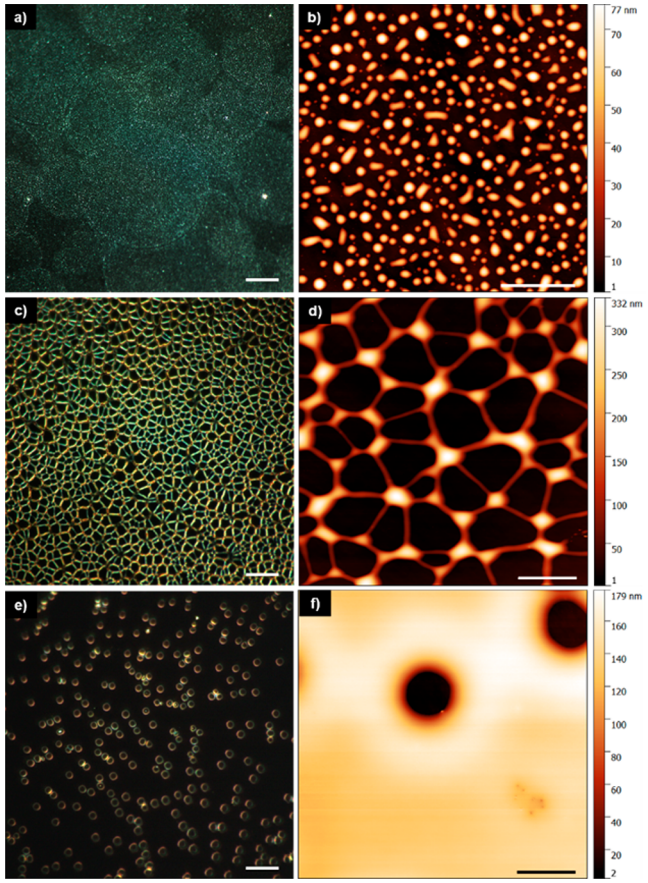

Figure 3. Dark field and corresponding AFM images of PLMA/QD films after dewetting with film thicknesses of (a,b) 9 nm, (c, d) 26 nm, and (e,f) 116 nm. Scale bars are 35 μm for the dark field images, 5 μm for (b), and 10 μm for (d) and (f).

DOI: 10.1021/acs.langmuir.7b03400
Langmuir 2017, 33, 14325−14331

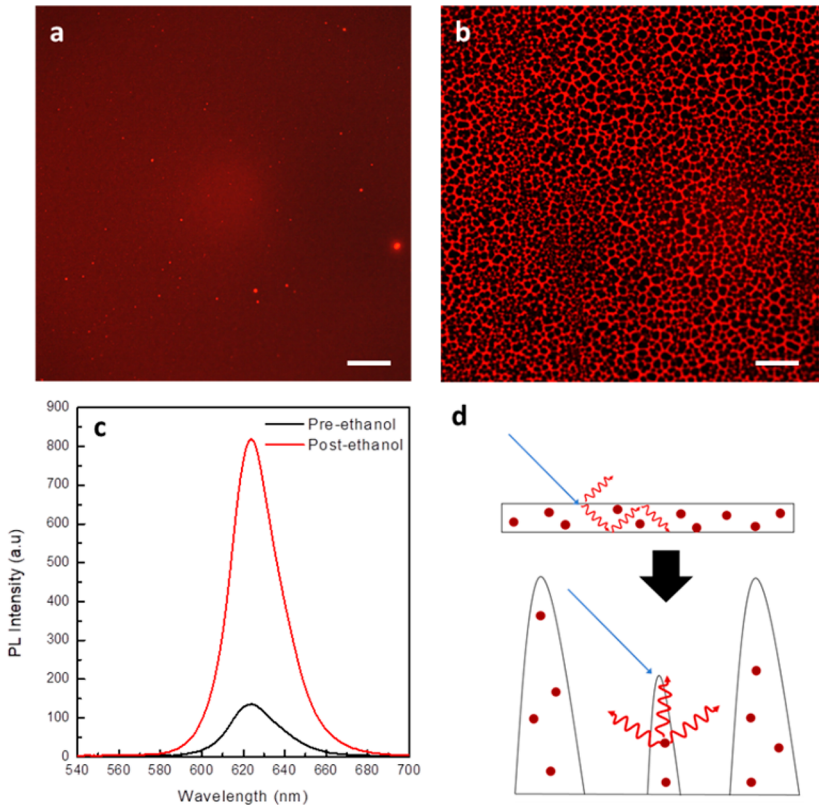

Figure 4. A 20 nm thick PLMA/QD thin film prior to dewetting. (b) Same 20 nm PLMA/QD film after dewetting. Scale bars are 35 μm. (c) PL intensity of films before and after ethanol treatment. (d) Proposed PL enhancement schematics.

3c,d and S1).[28,34] Such patterns arise due to the interfacial interactions between the film and the substrate along with differences in local film density, which lead to variations in the local effective Hamaker constant and areas of high conjoining pressure that the film flows to.[35] Due to the large thickness of these films and therefore the weaker energies between the film/substrate and film/ethanol interfaces, the hole nucleation process did not result in Rayleigh instability-formed droplets as seen in previous studies.[36] Maximum feature heights were seen to drastically increase after dewetting and were found to scale linearly with the initial film thickness (Figure S2). The dark field image of the 48 nm film also depicts several areas of the film that did not completely dewet, as evidenced by their lack of scattering despite the same Voronoi pattern elsewhere (Figure S1).

The 116 nm film exhibited little dewetting, and ethanol vapor exposure only resulted in the random formation of holes with a uniform diameter, which can be attributed to the much larger thickness of the film and consequently its higher resistance to dewetting. Such dewetting behavior is independent of the global dewetting processes attributed to spindoal decomposition or hole nucleation and are more indicative of local defect nucleation.[29] In this case, the excess composite material is not driven to areas of high conjoining pressure but instead deposits as rims around the holes (Figure 3e,f).

For all PLMA/QD films, it should be noted that the volume of the films stayed approximately the same before and after the dewetting process as estimated from AFM-calculated volumes after dewetting (Figure S3). Indeed, the volumes calculated for the dewetted films are slightly larger for every film thickness than before dewetting, which can be attributed to the influence of the AFM tip convolution. Importantly, this observation indicates that no PLMA/QD film material is irreverisbly lost during the dewetting process.

The dewetted 9, 20, and 26 nm films also exhibited increasing respective characteristic length scales of their network structures of 1.2, 4.8, and 8.3 μm as derived from the FFT transformation of the AFM images. Apart from confirming a feature size increase with a corresponding initial film thickness increase, the characteristic lengths are seen to scale linearly similarly to the maximum size of the individual domains. The 48 nm film however featured a similar characteristic length to that of the 26 nm film of 8.2 μm. This observation may indicate a maximum feature size of the dewetting process as controlled by the local dewetting dynamics above a critical film thickness. Further initial film thickness increases beyond this critical limit result solely in the inhibition of dewetting and preservation of the initial film uniformity, as seen with the 48 nm film dark field image (Figure S1).

Dewetting-Induced Photoluminescent Enhancement. Upon exposure to ethanol vapor, the drastic film morphology changes seen in scattering affect the PL properties as well (Figure 4a,b). It is apparent that the regions that correspond to high amounts of light scattering as observed in dark field also correlate with local high PL intensity. While the drastically increased brightness of the scattering sites can partially be attributed to higher volumes of material in these areas, the average PL intensity is higher than that before dewetting as well. For instance, the same 20 nm thick PLMA/QD film shows much different PL values before and after dewetting (Figure 4c).

The mechanism behind this enhancement is proposed to be a reduction of internal waveguiding within the film and a

DOI: 10.1021/acs.langmuir.7b03400
Langmuir 2017, 33, 14325−14331

corresponding increase in light scattering that result in improved far-field outcoupling (Figure 4d). Thin emissive films with large refractive index differences from those of the medium and the substrate are likely to possess total internal waveguiding modes due to classical optical effects (total internal reflection from Snell's law) and high reabsorption losses.[25,37,38] Indeed, previous studies have demonstrated the effectiveness of polymer/QD composites for waveguiding within their films and fibers even under the least ideal case of excitation with a normal angle of incidence.[39,40] By introducing scattering sites within the film, waveguided modes can be partially eliminated and an increase in apparent brightness can be achieved.

To ensure that no other variables were causing a change in the PL, two different excitation wavelengths of 492 and 572 nm were used to determine whether the absorption of the polymer at specific wavelengths was a factor in the observed enhancement (Figure S4). For both excitation wavelengths, PL enhancement occurred after dewetting and was similar in the magnitude of enhancement. To determine if ethanol exposure intrinsically modified the QDs, a a pure film of QDs was exposed to ethanol vapor in the same manner and did not display any notable PL enhancement (Figure S5). Therefore, the enhancement is proven to be solely a factor of the polymer reconfiguration. The scattering spectra of the dewet PLMA/QD films are also not spectrally engineered to overlap with the QD emission, as is required for photonic crystal enhancement, and are broadband in nature as well, meaning this process can be facilely applied to many different systems and materials with different emission wavelengths.

The effect of composite film thickness on the dewetting-induced photoluminescent enhancement can be seen in Figure 5. The 9, 20, 26, 48, and 116 nm PLMA/QD film PL intensities were measured both before and after dewetting from five different spots for each film, and corresponding PL enhancement factors of approximately 3-, 4-, 5-, 2-, and 1-fold were obtained. Composite film thicknesses of 9, 20, and 26 nm are seen to exhibit the largest PL enhancements upon dewetting, as thicker films do not dewet completely from the surface and consequently exhibit lower amounts of scattering (Figure S6). The 116 nm film exhibited very little surface reorganization upon ethanol vapor exposure as seen in Figure 3e and consequently demonstrated virtually no PL enhancement. This variation in the dewetting behavior also resulted in larger PL enhancement variability for the 48 and 116 nm films, as seen by their corresponding intrasample standard deviations (Figure 5a).

The loading of the QDs in a PLMA/QD film with a fixed film thickness was also seen to affect the PL enhancement properties (Figure 5b). In a 0.5 wt % PLMA solution, QDs were loaded with concentrations of 1.56, 3.12, 4.69, 6.25, and 12.5 mg/mL. Composite films with higher QD loadings were found to benefit less from the dewetting-induced polymer reconfiguration, with average enhancement factors being 3−5 for concentrations below 6.25 mg/mL and 2−2.5 for 6.25 and 12.5 mg/mL. Most likely, composite films with higher loadings exhibit naturally larger amounts of scattering due to an increased number of QD aggregates in the as-spun films and thus benefit less from the dewetting process, although the outcoupling enhancement is still notable.

Dewetting-Based Photopatterning. Because the PL enhancement is correlated with the dewetting behavior of the film, one can pattern areas of enhanced PL by modifying the film adhesion strength with the substrate. One possible route is by exposing films to light through a photopattern mask (Figure 6a). This process is able to selectively modify the polymer layer by light absorption in a manner analogous to polymer resist baking by removing residual solvent and promoting surface adhesion.[41] Direct high temperature baking processes were avoided due to the possibility of creating defects in the QDs at high temperatures and the limited spatial resolution achievable by thermal annealing and baking methods.

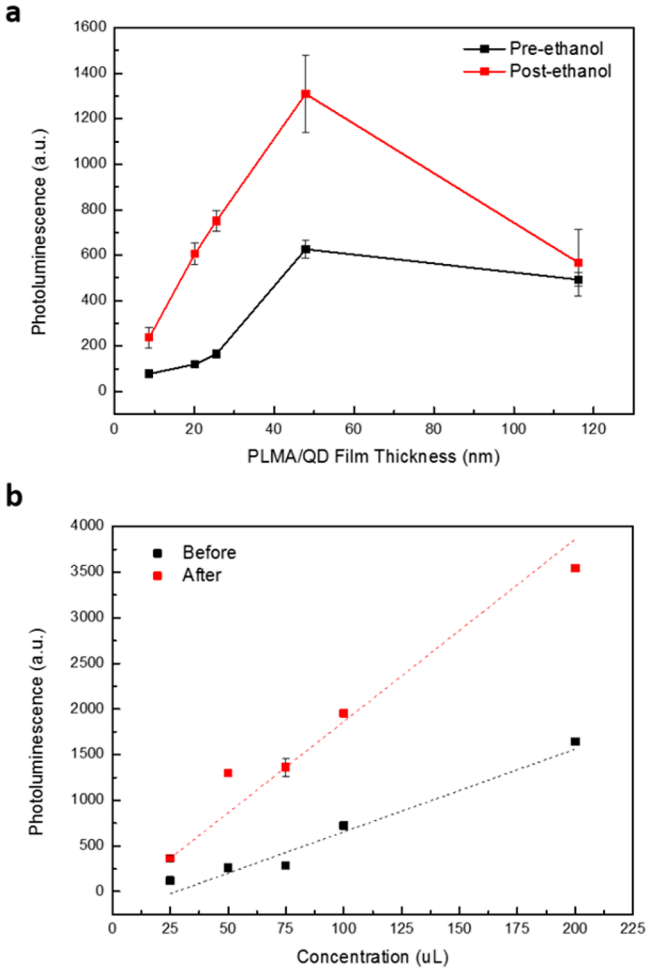

Figure 5. (a) PL as a function of initial PLMA/QD film thickness, with the concentration of QDs fixed. (b) PL as a function of the QD concentration, with the initial PLMA/QD film thickness fixed.

Directly after light exposure, patterned areas of the film exhibited no PL enhancement or reduction, signifying that the QDs themselves are stable enough to remain unaffected by the exposure process. In contrast, less stable QDs such as CdSe/ZnS core/shell QDS have exhibited PL enhancement after light exposure due to defect passivation mechanisms.[42,43] It should however be noted that PL enhancement of QDs in this manner is short-lived and that continued exposure of QDs to light results in PL decay due to photooxidation of the shell and the formation of surface traps.[43] After ethanol vapor exposure, the photopattern was successfully replicated in a negative manner, with exposed areas exhibiting lower amounts of PL (Figure 6b). The photopattern was also found to be replicated in dark field microscopy, further confirming that the patterning is not due to intrinsic modification of the QDs (Figure 6c). Finally, AFM images confirm that dewetting-induced hole nucleation is

DOI: 10.1021/acs.langmuir.7b03400
Langmuir 2017, 33, 14325−14331

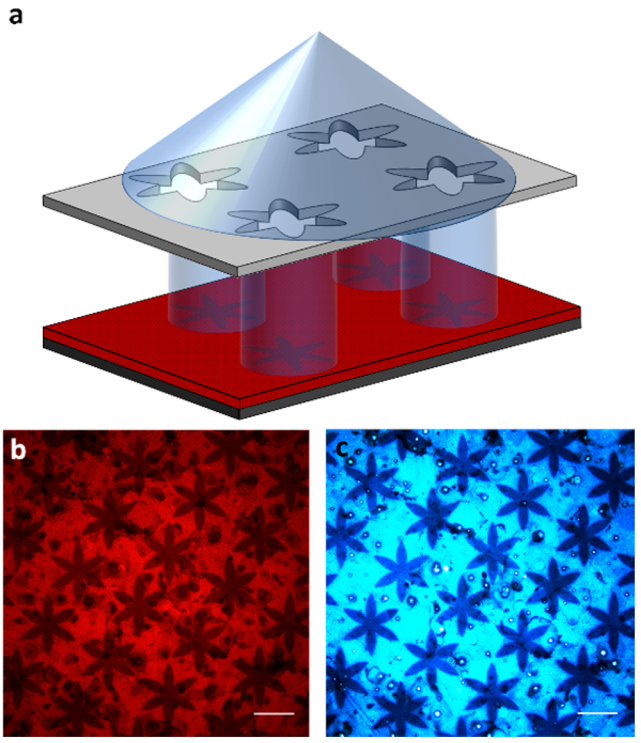

Figure 6. (a) Schematic of the PLMA/QD photopatterning process. (b) PL image of a PLMA/QD film after photopatterning. (c) Dark field microscopy of the same area. Scale bars are 200 μm.

greatly reduced in the areas that were exposed to light (Figure S7). It is believed that the photoexposure process therefore reduces the polymer chain mobility and prevents the drastic reconfiguration seen for unmodified PLMA/QD films upon exposure to ethanol.

CONCLUSIONS

The controlled dewetting of PLMA/QD composite thin films was demonstrated to result in large PL enhancement factors. Ultimately, enhancement factors of up to 5 for PLMA/QD thin films were demonstrated, and it was shown that enhancement is possible for a wide range of film thicknesses and QD concentrations. The primary enhancement effect is attributed to the creation of scattering sites within the films upon nonsolvent exposure, which consequently disrupts internal waveguiding modes and increases PL outcoupling. Importantly, this method can be used to facilely enhance many polymer/QD composite thin films without the need for complicated fabrication processes or precise coupling parameters.

Photopatterning was additionally demonstrated to be feasible in patterning areas of film adhesion and dewetting, which consequently led to specifically selected areas of PL enhancement. Finally, it is worth noting that this dewetting-induced enhancement process avoids the need for specific spectral overlaps, as in the case of photonic crystal or plasmonic systems, and it can be conducted easily in a quick and large-scale manner. It should be noted that this patterning method is currently limited to micrometer-size features without further modifications that would shrink the dewetted film characteristic length scale. One significant benefit to this photopatterning process, in comparison to many photomasking techniques, is that no prior masking or templating needs to be done with a sacrificial layer, thereby reducing the complexity of the patterning process. Overall, the outcoupling enhancement of QD thin films is highly relevant for many optoelectronic applications such as LEDs,[41] displays,[42] and lasers.[43]

ASSOCIATED CONTENT

Supporting Information

The Supporting Information is available free of charge on the ACS Publications website at DOI: 10.1021/acs.langmuir.7b03400.

PLMA/QD composite film morphologies; maximum feature height of dewet QD/PLMA films as a function of film thickness before dewetting; volume of QD/PLMA films before and after dewetting as measured by AFM; PL of a QD/PLMA film excited with 492 and 572 nm light before and after dewetting; PL of a pure QD film before and after exposure to ethanol; scattering spectra of 0.25, 0.5, 0.75, 1, and 2 wt % PLMA/QD composite films after dewetting; AFM image of a photopatterned star tip after the PLMA/QD dewetting process (PDF)

AUTHOR INFORMATION

Corresponding Author

*E-mail: vladimir@mse.gatech.edu.

ORCID

Zhiqun Lin: 0000-0003-3158-9340

Vladimir V. Tsukruk: 0000-0001-5489-0967

Notes

The authors declare no competing financial interest.

ACKNOWLEDGMENTS

This work was supported by the U.S. Department of Energy, Office of Basic Energy Sciences, Division of Materials Sciences and Engineering under Award #DE-FG02-09ER46604. The synthesis of quantum dots was conducted with financial support from the Air Force Office of Scientific Research FA9550-14-1-0037 (synthetic photonics Multidisciplinary University Research Initiative: synthesis, fabrication, and development).

REFERENCES

(1) Murphy, C. J. Peer Reviewed: Optical Sensing with Quantum Dots. *Anal. Chem.* **2002**, *74*, 520A−526A.

(2) Algar, W. R.; Susumu, K.; Delehanty, J. B.; Medintz, I. L. Semiconductor Quantum Dots in Bioanalysis: Crossing the Valley of Death. *Anal. Chem.* **2011**, *83*, 8826−8837.

(3) Medintz, I. L.; Uyeda, H. T.; Goldman, E. R.; Mattoussi, H. Quantum dot bioconjugates for imaging, labelling and sensing. *Nat. Mater.* **2005**, *4*, 435−446.

(4) Bimberg, D.; Grundmann, M.; Ledentsov, N. N. *Quantum dot heterostructures*; John Wiley & Sons: 1999.

(5) Dabbousi, B. O.; Rodriguez-Viejo, J.; Mikulec, F. V.; Heine, J. R.; Mattoussi, H.; Ober, R.; Jensen, K. F.; Bawendi, M. G. (CdSe)ZnS Core−Shell Quantum Dots: Synthesis and Characterization of a Size Series of Highly Luminescent Nanocrystallites. *J. Phys. Chem. B* **1997**, *101*, 9463−9475.

(6) Dennis, A. M.; Mangum, B. D.; Piryatinski, A.; Park, Y.-S.; Hannah, D. C.; Casson, J. L.; Williams, D. J.; Schaller, R. D.; Htoon, H.; Hollingsworth, J. A. Suppressed blinking and Auger recombination in near-infrared type-II InP/CdS Nanocrystal Quantum Dots. *Nano Lett.* **2012**, *12*, 5545−5551.

(7) Lin, C.; Lafalce, E.; Jung, J.; Smith, M. J.; Malak, S. T.; Aryal, S.; Yoon, J.; Zhai, Y.; Lin, Z.; Vardeny, V.; Tsukruk, V. V. Core/alloyed-

shell quantum dot robust solid films with high optical gains. *ACS Photonics* **2016**, *3*, 647−658.
(8) Greytak, A. B.; Allen, P. M.; Liu, W.; Zhao, J.; Young, E. R.; Popović, Z.; Walker, B. J.; Nocera, D. G.; Bawendi, M. G. Alternating layer addition approach to CdSe/CdS core/shell quantum dots with near-unity quantum yield and high on-time fractions. *Chem. Sci.* **2012**, *3*, 2028−2034.
(9) Bruchez, M.; Moronne, M.; Gin, P.; Weiss, S.; Alivisatos, A. P. Semiconductor nanocrystals as fluorescent biological labels. *Science* **1998**, *281*, 2013−2016.
(10) Caruge, J.; Halpert, J.; Wood, V.; Bulović, V.; Bawendi, M. Colloidal quantum-dot light-emitting diodes with metal-oxide charge transport layers. *Nat. Photonics* **2008**, *2*, 247−250.
(11) Zhao, J.; Bardecker, J. A.; Munro, A. M.; Liu, M. S.; Niu, Y.; Ding, I.-K.; Luo, J.; Chen, B.; Jen, A. K.-Y.; Ginger, D. S. Efficient CdSe/CdS quantum dot light-emitting diodes using a thermally polymerized hole transport layer. *Nano Lett.* **2006**, *6*, 463−467.
(12) Nozik, A. Quantum dot solar cells. *Phys. E* **2002**, *14*, 115−120.
(13) Park, G.; Shchekin, O. B.; Huffaker, D. L.; Deppe, D. G. Low-threshold oxide-confined 1.3-μm quantum-dot laser. *IEEE Photonics Technol. Lett.* **2000**, *12*, 230−232.
(14) Ganesh, N.; Zhang, W.; Mathias, P. C.; Chow, E.; Soares, J. A. N. T.; Malyarchuk, V.; Smith, A. D.; Cunningham, B. T. Enhanced fluorescence emission from quantum dots on a photonic crystal surface. *Nat. Nanotechnol.* **2007**, *2*, 515−520.
(15) Tan, Y.; Sutanto, E.; Alleyne, A. G.; Cunningham, B. T. Photonic crystal enhancement of a homogeneous fluorescent assay using submicron fluid channels fabricated by E-jet patterning. *J. Biophotonics* **2014**, *7*, 266−275.
(16) See, G. G.; Naughton, M. S.; Xu, L.; Nuzzo, R. G.; Kenis, P. J. A.; Cunningham, B. T. Enhanced emission of quantum dots embedded within the high-index dielectric regions of photonic crystal slabs. *Appl. Phys. Lett.* **2016**, *108*, 171108.
(17) Pompa, P.; Martiradonna, L.; Della Torre, A.; Della Sala, F.; Manna, L.; De Vittorio, M.; Calabi, F.; Cingolani, R.; Rinaldi, R. Metal-enhanced fluorescence of colloidal nanocrystals with nanoscale control. *Nat. Nanotechnol.* **2006**, *1*, 126−130.
(18) Aslan, K.; Wu, M.; Lakowicz, J. R.; Geddes, C. D. Fluorescent core− shell Ag@ SiO2 nanocomposites for metal-enhanced fluorescence and single nanoparticle sensing platforms. *J. Am. Chem. Soc.* **2007**, *129*, 1524−1525.
(19) Akselrod, G. M.; Argyropoulos, C.; Hoang, T. B.; Ciracì, C.; Fang, C.; Huang, J.; Smith, D. R.; Mikkelsen, M. H. Probing the mechanisms of large Purcell enhancement in plasmonic nanoantennas. *Nat. Photonics* **2014**, *8*, 835−840.
(20) Hoang, T. B.; Akselrod, G. M.; Argyropoulos, C.; Huang, J.; Smith, D. R.; Mikkelsen, M. H. Ultrafast spontaneous emission source using plasmonic nanoantennas. *Nat. Commun.* **2015**, *6*, 7788.
(21) Nepal, D.; Drummy, L. F.; Biswas, S.; Park, K.; Vaia, R. A. Large scale solution assembly of quantum dot−gold nanorod architectures with plasmon enhanced fluorescence. *ACS Nano* **2013**, *7*, 9064−9074.
(22) Karvinen, P.; Nuutinen, T.; Rahomäki, J.; Hyvärinen, O.; Vahimaa, P. Strong fluorescence-signal gain with single-excitation-enhancing and emission-directing nanostructured diffraction grating. *Opt. Lett.* **2009**, *34*, 3208−3210.
(23) Pan, Y.-L.; Hill, S. C.; Wolf, J.-P.; Holler, S.; Chang, R. K.; Bottiger, J. R. Backward-enhanced fluorescence from clusters of microspheres and particles of tryptophan. *Appl. Opt.* **2002**, *41*, 2994−2999.
(24) Derkacs, D.; Chen, W.; Matheu, P.; Lim, S.; Yu, P.; Yu, E. Nanoparticle-induced light scattering for improved performance of quantum-well solar cells. *Appl. Phys. Lett.* **2008**, *93*, 091107.
(25) Prins, F.; Kim, D. K.; Cui, J.; De Leo, E.; Spiegel, L. L.; McPeak, K. M.; Norris, D. J. Direct Patterning of Colloidal Quantum-Dot Thin Films for Enhanced and Spectrally Selective Out-Coupling of Emission. *Nano Lett.* **2017**, *17*, 1319−1325.
(26) Reiter, G.; Sharma, A.; Casoli, A.; David, M.-O.; Khanna, R.; Auroy, P. Thin Film Instability Induced by Long-Range Forces. *Langmuir* **1999**, *15*, 2551−2558.
(27) Xu, L.; Sharma, A.; Joo, S. W. Dewetting of Stable Thin Polymer Films Induced by a Poor Solvent: Role of Polar Interactions. *Macromolecules* **2012**, *45*, 6628−6633.
(28) Reiter, G. Dewetting of thin polymer films. *Phys. Rev. Lett.* **1992**, *68*, 75−78.
(29) Seemann, R.; Herminghaus, S.; Jacobs, K. Dewetting Patterns and Molecular Forces: A Reconciliation. *Phys. Rev. Lett.* **2001**, *86*, 5534−5537.
(30) Xue, L.; Han, Y. Autophobic Dewetting of a Poly(methyl methacrylate) Thin Film on a Silicon Wafer Treated in Good Solvent Vapor. *Langmuir* **2009**, *25*, 5135−5140.
(31) Verma, A.; Sekhar, S.; Sachan, P.; Reddy, P. D. S.; Sharma, A. Control of Morphologies and Length Scales in Intensified Dewetting of Electron Beam Modified Polymer Thin Films under a Liquid Solvent Mixture. *Macromolecules* **2015**, *48*, 3318−3326.
(32) Jung, J.; Lin, C. H.; Yoon, Y. J.; Malak, S. T.; Zhai, Y.; Thomas, E. L.; Vardeny, Z. V.; Tsukruk, V. V.; Lin, Z. Crafting Core/Graded Shell/Shell Quantum Dots with Suppressed Re-absorption and Tunable Stokes Shift as High Optical Gain Materials. *Angew. Chem., Int. Ed.* **2016**, *55*, 5071−5075.
(33) McConney, M. E.; Singamaneni, S.; Tsukruk, V. V. Probing Soft Matter with the Atomic Force Microscopies: Imaging and Force Spectroscopy. *Polym. Rev.* **2010**, *50*, 235−286.
(34) Kim, H. I.; Mate, C. M.; Hannibal, K. A.; Perry, S. S. How Disjoining Pressure Drives the Dewetting of a Polymer Film on a Silicon Surface. *Phys. Rev. Lett.* **1999**, *82*, 3496−3499.
(35) Xue, L.; Han, Y. Inhibition of dewetting of thin polymer films. *Prog. Mater. Sci.* **2012**, *57*, 947−979.
(36) Sharma, A.; Reiter, G. Instability of Thin Polymer Films on Coated Substrates: Rupture, Dewetting, and Drop Formation. *J. Colloid Interface Sci.* **1996**, *178*, 383−399.
(37) Nakamura, T.; Tsutsumi, N.; Juni, N.; Fujii, H. Thin-film waveguiding mode light extraction in organic electroluminescent device using high refractive index substrate. *J. Appl. Phys.* **2005**, *97*, 054505.
(38) Greenham, N. C.; Friend, R. H.; Bradley, D. D. C. Angular Dependence of the Emission from a Conjugated Polymer Light-Emitting Diode: Implications for efficiency calculations. *Adv. Mater.* **1994**, *6*, 491−494.
(39) Liu, H.; Edel, J. B.; Bellan, L. M.; Craighead, H. G. Electrospun Polymer Nanofibers as Subwavelength Optical Waveguides Incorporating Quantum Dots. *Small* **2006**, *2*, 495−499.
(40) Suárez, I.; Gordillo, H.; Abargues, R.; Albert, S.; Martínez-Pastor, J. Photoluminescence waveguiding in CdSe and CdTe QDs−PMMA nanocomposite films. *Nanotechnology* **2011**, *22*, 435202.
(41) Thompson, L. F.; Kerwin, R. E. Polymer Resist Systems for Photo- And Electron Lithography. *Annu. Rev. Mater. Sci.* **1976**, *6*, 267−301.
(42) Wang, Y.; Tang, Z.; Correa-Duarte, M. A.; Liz-Marzán, L. M.; Kotov, N. A. Multicolor Luminescence Patterning by Photoactivation of Semiconductor Nanoparticle Films. *J. Am. Chem. Soc.* **2003**, *125*, 2830−2831.
(43) Malak, S. T.; Jung, J.; Yoon, Y. J.; Smith, M. J.; Lin, C. H.; Lin, Z.; Tsukruk, V. V. Large-Area Multicolor Emissive Patterns of Quantum Dot−Polymer Films via Targeted Recovery of Emission Signature. *Adv. Opt. Mater.* **2016**, *4*, 608−619.

DOI: 10.1021/acs.langmuir.7b03400
Langmuir 2017, 33, 14325−14331